PHYSICAL REVIEW B **92**, 121407(R) (2015)

Kerr nonlinearity and plasmonic bistability in graphene nanoribbons

Thomas Christensen,[1,2] Wei Yan,[1,2] Antti-Pekka Jauho,[2,3] Martijn Wubs,[1,2] and N. Asger Mortensen[1,2,*]

[1]*Department of Photonics Engineering, Technical University of Denmark, DK-2800 Kgs. Lyngby, Denmark*

[2]*Center for Nanostructured Graphene, Technical University of Denmark, DK-2800 Kgs. Lyngby, Denmark*

[3]*Department of Micro- and Nanotechnology, Technical University of Denmark, DK-2800 Kgs. Lyngby, Denmark*

(Received 8 June 2015; published 16 September 2015)

We theoretically examine the role of Kerr nonlinearities for graphene plasmonics in nanostructures, specifically in nanoribbons. The nonlinear Kerr interaction is included semiclassically in the intraband approximation. The resulting electromagnetic problem is solved numerically by self-consistent iteration with linear steps using a real-space discretization. We derive a simple approximation for the resonance shifts in general graphene nanostructures, and obtain excellent agreement with numerics for moderately high field strengths. Near plasmonic resonances the nonlinearities are strongly enhanced due to field enhancement, and the total nonlinearity is significantly affected by the field inhomogeneity of the plasmonic excitation. Finally, we discuss the emergence of a plasmonic bistability which exists for energies red-shifted relative to the linear resonance. Our results offer insights into the role of nonlinear interaction in nanostructured graphene and pave the way for experimental investigation.

DOI: 10.1103/PhysRevB.92.121407 PACS number(s): 78.67.Wj, 73.20.Mf, 78.20.Ci, 78.20.Mg

Nonlinear optical effects [1,2], facilitated by strong light-matter interaction, are indispensable in modern photonics. Indeed, a host of phenomena and applications arise at sufficiently high field strengths, owing to superlinear photon-photon response mediated by strong light-matter interaction, ranging from frequency conversion through all-optical phase modulation to ultrafast switching, and is pursued in a broad range of platforms [3–5]. A perennial challenge in the discipline is to achieve significant nonlinear interaction at ever smaller excitation powers and interaction volumes, while maintaining *in situ* tunability and control. In achieving this goal, the field of plasmonics, describing the strong hybridization of the free electromagnetic field with collective oscillations of conduction electrons, suggests several promising avenues [6]. In particular, the extreme local field enhancements inherent to plasmonic excitations amplify intrinsic nonlinearities considerably, allowing large effective nonlinearities.

Nevertheless, plasmonic field enhancement is fundamentally limited by intrinsic Ohmic losses even in noble metals. The advent of the two-dimensional material graphene has garnered significant interest in the plasmonic community [7–10], in part due to extremely large electron mobilities [11–13] and concomitant extraordinary plasmonic field enhancements [14], exceeding even the very large enhancements known from metal plasmonics. Furthermore, graphene has attracted much interest also for its exceptional intrinsic nonlinear properties both theoretically [15–18] and experimentally [19–21]. Building on this compound fortuity, a body of research is rapidly emerging at the crossroad of nonlinear plasmonics and graphene [22–32].

Very recently, the role of Kerr nonlinearities in infinitely extended graphene has been studied, notably establishing the existence of bistable [22] and soliton solutions [23–25]. In this Rapid Communication, we study theoretically an analogous Kerr nonlinearity but in nanostructured graphene, specifically in nanoribbons, wherein plasmons, unlike in the extended counterpart, are readily excited without momentum-matching concerns, e.g., by normally incident plane waves. We report an induced nonlinearity which is significantly affected by the degree of inhomogeneity of the electric fields of the plasmon, a feature which is absent in the corresponding extended system [22] or in coupled-dipole treatments [25]. Furthermore, we derive a simple perturbative expression for the nonlinear resonance shifts in general graphene nanostructures, which agrees excellently with full self-consistent calculations for moderately high field strengths and also explains recent numerical considerations of nonlinear ribbon notch filters [26]. Finally, we discuss the emergence of plasmonic bistability in nanoribbons under plane-wave excitation. First, however, we introduce the two components needed for a nonlinear treatment of graphene nanostructures, namely, a material response model and an exposition of the resulting electromagnetic problem.

Material response. For photon energies $\hbar\omega$ below the Fermi energy ϵ_{F}, the response of graphene is reasonably approximated by neglecting interband transitions. In this case, the intraband response can be derived from the Boltzmann equation. To third order in the perturbing field, the Kerr-corrected conductivity, i.e., the response oscillating at the perturbing frequency, is [22]

$$\sigma(\mathbf{r}) = \sigma_{(1)}\big[1 - |\mathbf{E}(\mathbf{r})|^2/E_{(3)}^2\big], \tag{1}$$

expressed in terms of the linear intraband conductivity $\sigma_{(1)} = ie^2\epsilon_{\mathrm{F}}/\pi\hbar^2(\omega + i\gamma)$ with loss rate γ, and a third-order characteristic field $E_{(3)}^2 \equiv (8\varpi_{(3)}^2)/(9\omega^2)E_{\mathrm{sat}}^2$ linearly related to the saturation field $E_{\mathrm{sat}} \equiv \epsilon_{\mathrm{F}}\omega/ev_{\mathrm{F}}$ through a loss-modified frequency $\varpi_{(3)}^2 \equiv (\omega + \frac{1}{2}i\gamma)(\omega - i\gamma)$. Since the Kerr correction is of the self-focusing type [30], its usage in finite structures with inhomogeneous fields must be augmented to include a saturating mechanism, or else suffer nonphysical runaway self-focusing [33]. Here, we adopt the well-known two-level saturation model or, in other words, the [0/2] Padé approximant of $\sigma(\mathbf{r})$ consistent with Eq. (1):

$$\sigma(\mathbf{r}) \simeq \frac{\sigma_{(1)}(\mathbf{r})}{1 + |\mathbf{E}(\mathbf{r})|^2/E_{(3)}^2} + \sigma_{(3)2\gamma}(\mathbf{r}). \tag{2}$$

*asger@mailaps.org

This model reproduces the third-order result of Eq. (1) in the $|\mathbf{E}(\mathbf{r})|/E_{\text{sat}} \ll 1$ limit, while crucially exhibiting a sensible behavior beyond this limit as well [34]. Lastly, we include in Eq. (2) a term $\sigma_{(3)2\gamma}(\mathbf{r})$ to account for a high field loss mechanism through two-photon absorption via the phenomenological prescription suggested by Gorbach [30], via the dissipative correction $\sigma_{(3)2\gamma}(\mathbf{r}) = -i\alpha_{2\gamma}\sigma_{(1)}|\mathbf{E}(\mathbf{r})|^2/E_{\text{sat}}^2$ with $\alpha_{2\gamma} \approx 0.1$ estimated from measurements [21].

Before proceeding, we briefly discuss the limitations of the material response assumed in Eq. (2). First, the disregard of interband effects limits our consideration to energies sufficiently below $\sim 2\epsilon_{\text{F}}$. Second, nonlocality [35], potential edge states [36], and more generally atomistic features [31,32,37,38] are excluded, although they are important at small feature sizes. Consequently, we restrict our considerations to nanostructures of characteristic dimensions $\gtrsim$25 nm where these effects only weakly perturb the intraband approximation.

Self-consistent response. In the quasistatic limit, the self-consistent response of graphene can be deduced from three elements: the Coulomb law, the continuity equation, and the current-field relationship as specified by a conductivity model. For a nanostructure defined by a two-dimensional domain Ω (e.g., at $z = 0$), these elements combine to form an integrodifferential equation for either the induced density or the total potential $\phi(\mathbf{r})$. Here, we choose the latter [8]:

$$\phi(\mathbf{r}) = \frac{i}{4\pi\varepsilon_0\omega W}\int_\Omega d^2\mathbf{r}'\, V(\mathbf{r},\mathbf{r}')\nabla'\cdot[\sigma(\mathbf{r}')\nabla'\phi(\mathbf{r}')], \quad (3)$$

expressed in dimensionless coordinates $\mathbf{r}^{(\prime)} = [x^{(\prime)}, y^{(\prime)}, z]^{\text{T}}$ normalized by a characteristic length W, with the Coulomb interaction $V(\mathbf{r},\mathbf{r}') = |\mathbf{r}-\mathbf{r}'|^{-1}$ [39], and with differential operators $\nabla' = [\partial_{x'}, \partial_{y'}]^{\text{T}}$. The conductivity $\sigma(\mathbf{r})$ implicitly depends on frequency and, in a nonlinear treatment, also on the total field $\mathbf{E}(\mathbf{r})$. The spatial dependence of the conductivity can be conveniently expressed via a dimensionless occupation function $f(\mathbf{r}) \equiv \sigma(\mathbf{r})/\langle\sigma_{(1)}\rangle$ with $\langle\sigma_{(1)}\rangle$ denoting the average linear conductivity across Ω. Introducing operators $\mathsf{V}g(\mathbf{r}) \equiv \int d\mathbf{r}' V(\mathbf{r},\mathbf{r}')g(\mathbf{r}')$ and $\mathsf{D}g(\mathbf{r}') \equiv \nabla'\cdot[f(\mathbf{r}')\nabla' g(\mathbf{r}')]$ casts Eq. (3) as an eigenvalue problem for the composite operator VD:

$$\lambda\phi(\mathbf{r}) = \mathsf{VD}\phi(\mathbf{r}), \quad (4)$$

with eigenvalues $\lambda \equiv 4\pi\varepsilon_0\omega W/i\langle\sigma_{(1)}\rangle$, dictating the permitted eigenenergies $\hbar\omega$. Operators V and D find simple matrix forms in a discretized real-space basis in both the general two-dimensional (2D) case as well as in the one-dimensional (1D) ribbon case [see Supplemental Material (SM) [40]]. A boundary condition of vanishing normal current at the boundary $\partial\Omega$ (or, equivalently, a discontinuous conductivity step) is incorporated explicitly in the construction of D. In the presence of an external potential ϕ_{ext}, the eigenvalue problem in Eq. (4) becomes an inhomogeneous equation through the addition to the right-hand side of a source term $\lambda\phi_{\text{ext}}(\mathbf{r})$. To solve the nonlinear problem, with $\sigma(\mathbf{r})$, and hence $f(\mathbf{r})$ and D, depending on the total electric field locally, we proceed iteratively until self-consistency is reached, exploiting at each iteration step the computational efficiency associated with linear systems [33] (see SM [40]).

With the formal premise established, we next specialize to the case of nanoribbons, translationally invariant along y and of finite extent W along x, a system which has already attracted much attention in the linear case [35,38,41,42]. As a consequence of translational symmetry, eigensolutions can be expanded in a momentum basis according to $\phi(\mathbf{r}) = \phi(x,z)\exp(ik_\parallel y)$. Of central interest is the evolution of the eigenenergies with momentum $k_\parallel$ (here dimensionless; conventional units via $k_\parallel/W$), i.e. the dispersion relation $\hbar\omega_n(k_\parallel)$, and subsequently the response of the system to external fields.

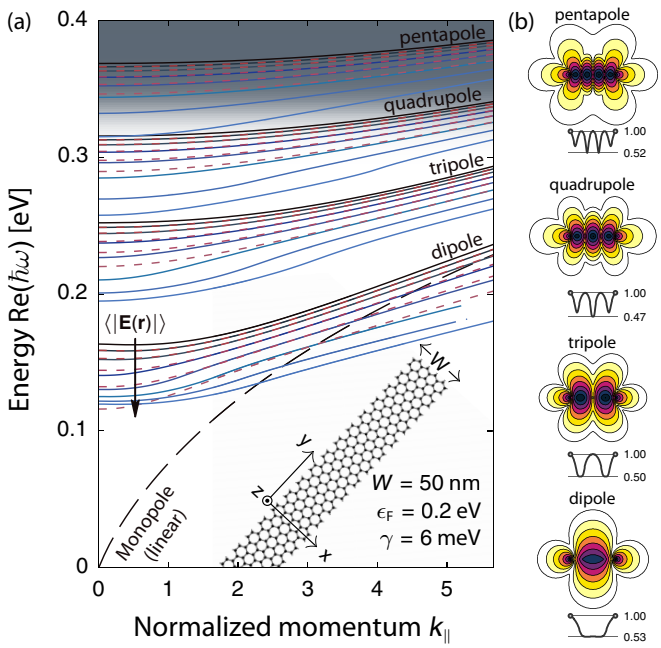

FIG. 1. (Color online) (a) Dispersion relation of a single nanoribbon. Ribbon-averaged field strength $\langle|\mathbf{E}(\mathbf{r})|\rangle$ ranges from negligible (black), i.e., linear, through 1×10^5 V/cm to 4×10^5 V/cm (lightest blue) in steps of 0.5×10^5 V/cm (increasing along arrow). For the first five $\langle|\mathbf{E}(\mathbf{r})|\rangle$, we indicate in dashed red the corresponding analytical estimate [see Eq. (5)]. For the monopole, only the linear calculation is shown. The region of significant interband modification is illustrated in shaded gray. Inset schematically depicts a single graphene nanoribbon. (b) Field amplitude $|\mathbf{E}(\mathbf{r})|$, contour maps for the case $\langle|\mathbf{E}(\mathbf{r})|\rangle = 4\times10^5$ V/cm, and $k_\parallel = 0$. Color map ranges from maximal (dark) to minimal (light) logarithmically, with contours separated by factors of 1.5, 1.75, 2, and 2.25 for dipole, tripole, quadrupole, and pentapole cases, respectively. Sparklines below maps depict the variation of $|f(\mathbf{r})|$ along the ribbon, with maximal and minimal values indicated; their widths equal that of the ribbon, thus indicating the spatial scale.

Eigenmodes and nonlinear dispersion. For low field strengths, i.e., in the linear regime with $f(\mathbf{r})$ independent of $\mathbf{E}(\mathbf{r})$, the eigenmodes $\lambda_n(k_\parallel)$ of Eq. (4) are solely geometry dependent, but scale invariant, with associated eigenenergies $\hbar\omega_n(k_\parallel)$ dictated by $\lambda_n(k_\parallel) = 4\pi\varepsilon_0\omega_n(k_\parallel)W/i\langle\sigma_{(1)}\rangle$, allowing in the linear intraband approximation the simple scaling relation $\hbar\omega_n(k_\parallel) \simeq (2\pi)^{-1}\sqrt{-\lambda_n(k_\parallel)e^2\epsilon_{\text{F}}/\varepsilon_0 W}$ [35,41]. Under significant nonlinear interaction, however, the eigenvalues $\lambda_n(k_\parallel)$ are field dependent and, by extension, scale dependent due to the self-consistent nature of the problem. In Fig. 1(a), we investigate the dispersion relation of the first few eigenmodes of a single $W = 50$ nm nanoribbon for different ribbon-averaged field strengths $\langle|\mathbf{E}(\mathbf{r})|\rangle \equiv W^{-1}\int_\Omega dx|\mathbf{E}(x)|$.

The most apparent impact of nonlinearity is a red-shift of all resonances. This is readily appreciated from the negativity of the Kerr correction. Indeed, the shift can be well approximated by perturbation theory for any general structure: denoting by $\hbar\omega_n^{(0)}$ and $\mathbf{E}_n^{(0)}$ the *linear* response eigenenergies and eigenfields [with $\langle|\mathbf{E}_n^{(0)}(\mathbf{r})|\rangle = \langle|\mathbf{E}(\mathbf{r})|\rangle$] the nonlinear eigenenergies are, to lowest order, approximately (see SM [40])

$$\omega_n \simeq \omega_n^{(0)}\sqrt{1-\frac{9}{8}\frac{\langle|\mathbf{E}^{(0)}(\mathbf{r})|^4\rangle}{\langle|\mathbf{E}^{(0)}(\mathbf{r})|^2\rangle E_{\rm sat}^2}}, \tag{5}$$

with averages taken over $\mathbf{r}\in\Omega$. The approximation is excellent for moderately high fields [see dashed red lines of Fig. 1(a)], although, naturally, inadequate for the largest fields due to the disregard of the self-consistent aspects of the nonlinearity. The approximately linear relation between resonance shift and intensity recently discussed for nonlinear ribbon filters [26] is similarly captured by Eq. (5), thus adding new physical insight. Moreover, by introducing the inhomogeneity parameter $\kappa \equiv \langle|\mathbf{E}^{(0)}(\mathbf{r})|^4\rangle/\langle|\mathbf{E}^{(0)}(\mathbf{r})|^2\rangle^2$ ($\kappa \geqslant 1$, cf. the Cauchy-Schwarz inequality), Eq. (5) reveals that inhomogeneity both modifies and enhances the nonlinearity which is $\propto \kappa\langle|\mathbf{E}^{(0)}(\mathbf{r})|^2\rangle/E_{\rm sat}^2$.

In Fig. 1(b), we explore this point further by depicting the modal character and inhomogeneous nature of the plasmonic modes. The modal labels are chosen from the perspective of the induced charge density $\rho(x)$ of the nth mode, with the monopole, dipole, tripole, quadrupole, and pentapole ($n = 0,1,2,3$, and 4, respectively) exhibiting n nodes of $\rho(x)$. Modes of even n are optically dark, owing to a vanishing dipole moment, and remain optically dark also under nonlinear perturbations (which preserves the system symmetry). The monopole violates charge conservation along x [but not along (x,y) for $k_\parallel \neq 0$], is optically dark, and consistently does not converge at higher fields; as a consequence, we depict only its linear dispersion. The variation of the occupation function $f(\mathbf{r})$ under large fields is highlighted in the insets of Fig. 1(b). The pronounced spatial variation of $f(\mathbf{r})$, up to 50% for the considered $\langle|\mathbf{E}(\mathbf{r})|\rangle$, is a direct consequence of the strongly inhomogeneous nature of plasmons. Despite the significant variations of $f(\mathbf{r})$, the corresponding far-field mode profiles are highly similar in linear and nonlinear settings since they are dictated chiefly by the nodal character of $\rho(x)$.

Plane-wave excitation and bistability. Having considered the dispersion of eigenmodes, we next turn our attention to the response of the system due to a normally incident plane wave, polarized along x, i.e., $\mathbf{E}_{\rm ext}(z=0) = E_0\hat{\mathbf{x}}$ and $\phi_{\rm ext}(z=0) = -E_0 x W$, corresponding to vanishing $k_\parallel$. In addition to the power absorbed from the incident wave, the induced and total electric fields are of primary interest; here, we focus on the latter. For reasons of numerical efficiency and physical necessity, we compute for each separate energy the response by an initial linear calculation, followed by a ramping of the incident field strength first in upwards and then in downwards fashion, corresponding to a slow on-and-off turning of the maximum intensity; see SM [40] for implementational details.

In Fig. 2, we examine the spectral response of ribbons of widths $W = 25$ and 50 nm under different excitation strengths, i.e., under varying E_0. For moderately high E_0, the linear Lorentzian resonance is asymmetrically perturbed,

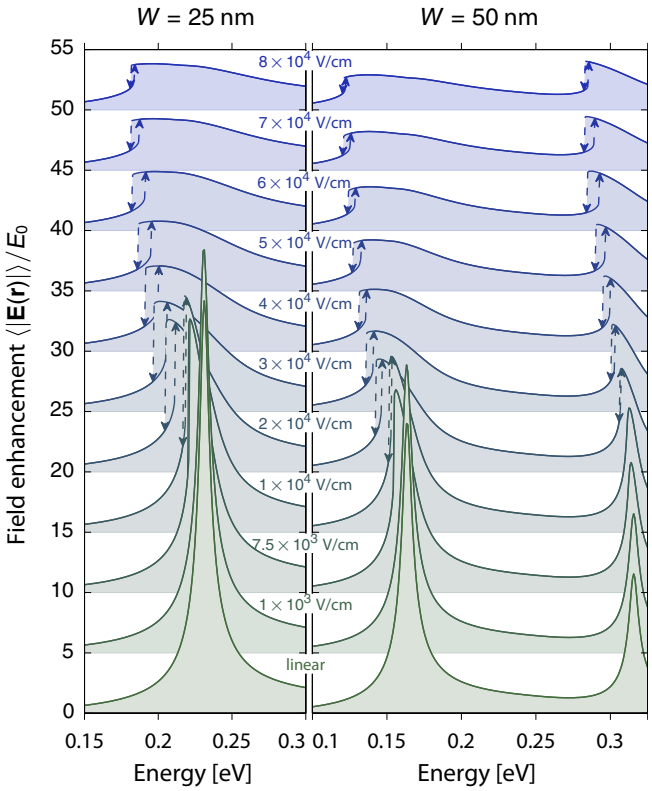

FIG. 2. (Color online) Field enhancement $\langle|\mathbf{E}(\mathbf{r})|\rangle/E_0$ as a function of energy $\hbar\omega$, for varying incident field strengths E_0 (as indicated above each spectrum). Each spectrum is offset vertically by five units. Two ribbon widths $W = 25$ and 50 nm are examined. Regions of bistability are delimited by dashed arrows which indicate the ramping direction. Material parameters are as in Fig. 1.

slightly broadened, and red-shifted. Furthermore, the upward and downward ramps to E_0 give identical spectra. As E_0 is increased further, these perturbations intensify. However, in certain energy ranges the response to upward and downward ramps toward E_0 differ (regions delimited by dashed arrows), a trademark of bistability. Similar features were found in Ref. [22] for extended graphene under normal incidence, in Ref. [25] for nanodisk chains in a coupled-dipole approximation, and in Ref. [31] for finite systems using a phenomenological anharmonic model. A key extension here is the full self-consistent accounting of the inhomogeneous nonlinear conductive profile arising in nanostructured systems. Also, coupling with the nanoribbon plasmons significantly expands the spectral region of bistability compared to the corresponding extended system under normal incidence (where plasmons are not excited), where it is restricted to $\hbar\omega < \sqrt{4/3}\alpha_{\rm fs}\epsilon_{\rm F}$ (with $\alpha_{\rm fs} \equiv e^2/4\pi\varepsilon_0\hbar c$) [22]. Here, bistability is evident in the dipole mode for both $W = 25$ and 50 nm, but also in the quadrupole mode for $W = 50$ nm. In both cases, the area traced by the bistable region initially increases with E_0 and then decreases due to mounting saturation and absorption.

The history dependence of the response is further examined in Fig. 3(b), depicting hysteresis curves of E_0 versus $\langle|\mathbf{E}(\mathbf{r})|\rangle$ at a selection of fixed energies as indicated in the linear spectrum of Fig. 3(a). At energies far from the linear resonance at $\hbar\omega^{(0)}$ the response $\langle|\mathbf{E}(\mathbf{r})|\rangle$ relates linearly with E_0. As the energy is

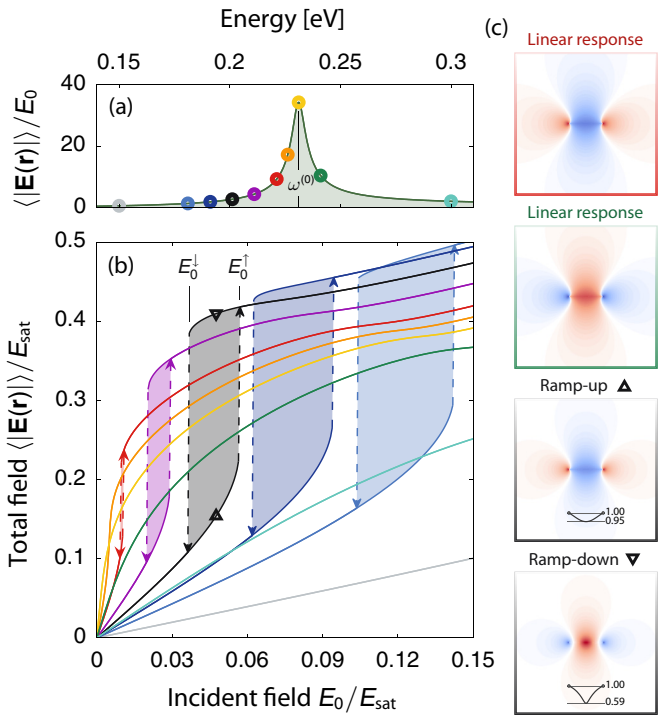

FIG. 3. (Color online) Hysteresis arising from bistable behavior in a $W = 25$ nm nanoribbon excited by a plane wave $E_0\hat{\mathbf{x}}$ (material parameters are as in Fig. 1). (a) Linear response field-enhancement spectrum. Selected energies are highlighted by colored markers, and the linear resonance energy $\hbar\omega^{(0)}$ is labeled. (b) Hysteresis curves at fixed energy [corresponding colorwise to those in (a)] for total field $\langle|\mathbf{E}(\mathbf{r})|\rangle$ versus incident field E_0. Bistable regions are indicated by shading and delimited by energy-dependent low- and high-point field strengths $E_0^{\downarrow\uparrow}$. (c) Intensity maps of the induced electric field $\mathrm{Re}[E_x^{\rm ind}(x,z)]$ in a 50×50 nm^2 cross-sectional region. Color scale is identical across the four maps, ranging from positive (red) through zero (white) to negative (blue) in a symmetric range. Absolute magnitudes are scaled logarithmically for intelligibility. Frame color indicates association with energies in (a). Field strengths in the high-field maps are specified by corresponding triangles in (b). Sparklines, defined as in Fig. 1(b), indicate the range and variation of $|f(\mathbf{r})|$.

increased towards $\hbar\omega^{(0)}$, a nonlinear discrepancy develops with increasing E_0 which eventually gives way to a discontinuous jump at a critical field strength $E_0^{\uparrow}$, indicated for a selected energy in Fig. 3(b). As E_0 is reduced on the downward ramp, its response initially traces out that of the upward ramp, but departs from its upward correspondent after $E_0^{\uparrow}$ and eventually undergoes a discontinuous jump at $E_0^{\downarrow}$ after which the initial path is retraced. The hysteresis area, indicated by shaded areas, increases with positive $\omega^{(0)} - \omega$ (although $E_0^{\uparrow}$ similarly increases, delaying the onset of hysteresis), but vanishes for $\omega \gtrsim \omega^{(0)}$ due to the red-shifting of the resonance with E_0. Due to plasmonic field enhancement of the total field, the onset of bistability is reached for incident field strengths considerably below $E_{\rm sat}$.

Lastly, we comment on the field profiles of the excitations. Specifically, we highlight the π phase shift that arises between the two bistable solutions in the black-framed maps. The phase shift can be appreciated from a simple anharmonic oscillator model [31], in partial analogy to the shift exhibited by the red- and green-framed maps of the linear resonance (see SM [40]).

Summary and discussion. In this Rapid Communication, we have analyzed the impact of Kerr nonlinearity on the plasmonic response of graphene nanostructures, specifically for nanoribbons. The key distinction of nanostructures compared to the corresponding extended system arises from the strongly inhomogeneous fields of localized plasmonic excitations, which in turn incur an inhomogeneous conductive profile. We have derived a simple analytic expression (5), which approximates the nonlinear resonance shifts, while accounting for both inhomogeneity and overall amplitude of the nonlinear perturbation. The characteristic field of the Kerr nonlinearity in graphene is the saturation field $E_{\rm sat}$. However, significant nonlinear interaction can be achieved near plasmonic resonances even for much weaker incident fields owing to plasmonic field enhancement. Finally, we discussed the existence of a plasmonic bistability in nanoribbons under normal incidence.

The applications of optical bistabilities are well known and long pursued [1,2], with implications particularly in optical switching. Indeed, a range of platforms have been scrutinized for this purpose, in recent years, e.g., in photonic crystal cavities (PCC) where nonlinearities are enhanced by large Q-factors and light slowdown [3]. Whether graphene can further the state of the art in this mature field remains to be seen [43]. We expect, however, that a very profitable avenue for progress exists in hybrid approaches, utilizing, e.g., PCC and graphene in unison, as has in fact been explored experimentally [21], albeit without taking advantage of the resonant plasmonic nonlinearity described herein. Advances in this direction require improved understanding of nonlinearities in nanostructures; this work constitutes one such effort. Several features, however, remain unexplored, underscoring the fertility and richness of the field. For example, from a semiclassical perspective, barring atomistic approaches [31,32], questions remain relating to the role of interband nonlinearities [18], nonlocality, and the effective role of edge states. The impact of substrate interactions, which affords, e.g., plasmon-phonon coupling [44,45], is similarly unexplored in nonlinear settings.

Penultimately, we highlight that graphene solitons, sustained by Kerr nonlinearities, also pose a number of intriguing opportunities [23–25]. Our present considerations actually generalize readily to treat temporal solitons through the 1D nonlinear Schrödinger equation. For instance, the group velocity dispersion and self-phase modulation parameters can be derived analytically in terms of $\lambda_n(k_\parallel)$ (see SM [40]). There, too, inhomogeneity has a pronounced impact.

In closing, we mention a final question of singular practical relevance, namely, damage thresholds. So far, to the best of our knowledge, measurements do not exist in the infrared, but in the optical domain [46–48] the reported thresholds fall in the rather broad range from $\sim 10^6$ V/cm in fs-pulsed operation [47] to just $\sim 10^4$ V/cm for hour-long continuous-wave operation [46], while technologically important substrates such as SiO_2 exhibit thresholds up to $\sim 10^8$ V/cm [49]. For comparison, the saturation field at $\hbar\omega = \epsilon_{\rm F} = 0.2$ eV is $E_{\rm sat} \approx 6.7 \times 10^5$ V/cm. Although direct comparison is impossible,

in part due to frequency range, pulse conditions, and the uncertain impact of field enhancement, this highlights that even resonantly enhanced nonlinearities in graphene walk a narrow road, not unlike previous contenders for large nonlinearities. Given the promising results presented herein, however, we believe the journey will be worth the effort.

The Center for Nanostructured Graphene is sponsored by the Danish National Research Foundation, Project No. DNRF58. This work was also supported by the Danish Council for Independent Research, Project No. 1323-00087. W.Y. acknowledges support from the Lundbeck Foundation, Grant No. 70802.

[1] R. W. Boyd, *Nonlinear Optics*, 3rd ed. (Academic, Burlington, MA, 2008).
[2] H. M. Gibbs, *Optical Instability: Controlling Light with Light* (Academic, New York, 1985).
[3] M. Soljačić and J. D. Joannopoulous, Nat. Mater. **3**, 211 (2004).
[4] J. M. Dudley and J. R. Taylor, Nat. Photonics **3**, 85 (2009).
[5] J. Leuthold, C. Koos, and W. Freude, Nat. Photonics **4**, 535 (2010).
[6] M. Kauranen and A. V. Zayats, Nat. Photonics **6**, 737 (2012).
[7] Y. V. Bludov, A. Ferreira, N. M. R. Peres, and M. I. Vasilevskiy, Int. J. Mod. Phys. B **27**, 1341001 (2013).
[8] F. J. García de Abajo, ACS Photonics **1**, 135 (2014).
[9] T. Stauber, J. Phys.: Condens. Matter **26**, 123201 (2014).
[10] T. Low and P. Avouris, ACS Nano **8**, 1086 (2014).
[11] K. S. Novoselov, A. K. Geim, S. V. Morozov, D. Jiang, Y. Zhang, S. V. Dubonos, I. V. Grigorieva, and A. A. Firsov, Science **306**, 666 (2004).
[12] K. I. Bolotin, K. J. Sikes, Z. Jiang, M. Klima, G. Fudenberg, J. Hone, P. Kim, and H. L. Stormer, Solid State Commun. **146**, 351 (2008).
[13] P. Tassin, T. Koschny, and C. M. Soukoulis, Science **341**, 620 (2013).
[14] S. Thongrattanasiri and F. J. García de Abajo, Phys. Rev. Lett. **110**, 187401 (2013).
[15] S. A. Mikhailov and K. Ziegler, J. Phys.: Condens. Matter **20**, 384204 (2008).
[16] S. A. Mikhailov, Physica E (Amsterdam) **44**, 924 (2012).
[17] X. Yao and A. Belyanin, Phys. Rev. Lett. **108**, 255503 (2012).
[18] J. L. Cheng, N. Vermeulen, and J. E. Sipe, New J. Phys. **16**, 053014 (2014).
[19] E. Hendry, P. J. Hale, J. Moger, A. K. Savchenko, and S. A. Mikhailov, Phys. Rev. Lett. **105**, 097401 (2010).
[20] H. Zhang, S. Virally, Q. Bao, L. K. Ping, S. Massar, N. Godbout, and P. Kockaert, Opt. Lett. **37**, 1856 (2012).
[21] T. Gu, N. Petrone, J. F. McMillan, A. van der Zande, M. Yu, G. Q. Lo, D. L. Kwong, J. Hone, and C. W. Wong, Nat. Photonics **6**, 554 (2012).
[22] N. M. R. Peres, Y. V. Bludov, J. E. Santos, A.-P. Jauho, and M. I. Vasilevskiy, Phys. Rev. B **90**, 125425 (2014).
[23] M. L. Nesterov, J. Bravo-Abad, A. Y. Nikitin, F. J. García-Vidal, and L. Martin-Moreno, Laser Photon. Rev. **7**, L7 (2013).
[24] D. A. Smirnova, I. V. Shadrivov, A. I. Smirnov, and Y. S. Kivshar, Laser Photon. Rev. **8**, 291 (2014).
[25] D. A. Smirnova, R. E. Noskov, L. A. Smirnov, and Y. S. Kivshar, Phys. Rev. B **91**, 075409 (2015).
[26] H. Nasari and M. S. Abrishamian, J. Opt. Soc. Am. B **31**, 1691 (2014).
[27] M. Gullans, D. E. Chang, F. H. L. Koppens, F. J. García de Abajo, and M. D. Lukin, Phys. Rev. Lett. **111**, 247401 (2013).
[28] X. Yao, M. Tokman, and A. Belyanin, Phys. Rev. Lett. **112**, 055501 (2014).
[29] D. A. Smirnova, I. V. Shadrivov, A. E. Miroshnichenko, A. I. Smirnov, and Y. S. Kivshar, Phys. Rev. B **90**, 035412 (2014).
[30] A. V. Gorbach, Phys. Rev. A **87**, 013830 (2013).
[31] J. D. Cox and F. J. García de Abajo, Nat. Commun. **5**, 5725 (2014).
[32] J. D. Cox and F. J. García de Abajo, ACS Photonics **2**, 306 (2015).
[33] X.-H. Wang, *Finite Element Methods for Nonlinear Optical Waveguides*, Advances in Nonlinear Optics Vol. 2 (Gordon and Breach, Amsterdam, 1995).
[34] Although the third-order term is recovered, the saturation model is in contradiction at the fifth order, whose Kerr contribution is $\sigma_{(5)} = -\sigma_{(1)}|\mathbf{E}|^4/E_{(5)}^4$ with $E_{(5)}^4 = (16\varpi_{(5)}^4)/(25\omega^4)E_{\rm sat}^4$ and $\varpi_{(5)}^4 \equiv \varpi_{(3)}^2(\omega + \frac{1}{3}i\gamma)(\omega - \frac{1}{2}i\gamma)$. This, however, can in principle be easily remedied by going to the [0/4] Padé approximant.
[35] W. Wang and J. M. Kinaret, Phys. Rev. B **87**, 195424 (2013).
[36] T. Christensen, W. Wang, A.-P. Jauho, M. Wubs, and N. A. Mortensen, Phys. Rev. B **90**, 241414(R) (2014).
[37] W. Wang, T. Christensen, A.-P. Jauho, K. S. Thygesen, M. Wubs, and N. A. Mortensen, Sci. Rep. **5**, 9535 (2015).
[38] I. Silveiro, J. M. P. Ortega, and F. J. García de Abajo, Light: Sci. Appl. **4**, e241 (2015).
[39] Rescaling $V(\mathbf{r},\mathbf{r}') \to \varepsilon_{\rm B}^{-1}V(\mathbf{r},\mathbf{r}')$ with $\varepsilon_{\rm B} \equiv \frac{1}{2}(\varepsilon_- + \varepsilon_+)$ accounts for nonunity and/or dispersive sub- and superstrates $\varepsilon_\pm(\omega)$.
[40] See Supplemental Material at http://link.aps.org/supplemental/10.1103/PhysRevB.92.121407 for a description of the iterative procedure applied the nonlinear problem, matrix representations of V and D for the nanoribbon, derivation of the perturbation approach, discussion of the qualitative anharmonic oscillator model, and a semianalytical treatment of plasmonic solitons.
[41] J. Christensen, A. Manjavacas, S. Thongrattanasiri, F. H. L. Koppens, and F. J. García de Abajo, ACS Nano **6**, 431 (2012).
[42] K. A. Velizhanin, Phys. Rev. B **91**, 125429 (2015).
[43] J. B. Khurgin, Appl. Phys. Lett. **104**, 161116 (2014).
[44] M. Freitag, T. Low, W. Zhu, H. Yan, F. Xia, and P. Avouris, Nat. Commun. **4**, 1951 (2013)
[45] X. Zhu, W. Wang, W. Yan, M. B. Larsen, P. Bøggild, T. G. Pedersen, S. Xiao, J. Zi, and N. A. Mortensen, Nano Lett. **14**, 2907 (2014).
[46] B. Krauss, T. Lohmann, D.-H. Chae, M. Haluska, K. von Klitzing, and J. H. Smet, Phys. Rev. B **79**, 165428 (2009).
[47] A. Roberts, D. Cormode, C. Reynolds, T. Newhouse-Illige, B. J. LeRoy, and A. S. Sandhu, Appl. Phys. Lett. **99**, 051912 (2011).
[48] M. Currie, J. D. Caldwell, F. J. Bezares, J. Robinson, T. Anderson, H. Chun, and M. Tadjer, Appl. Phys. Lett. **99**, 211909 (2011).
[49] W. H. Lowdermilk and D. Milam, IEEE J. Quantum Electron. **17**, 1888 (1981).